A Review on Personalized Pediatric Dosimetry Applications Using Advanced Computational Tools

Panagiotis Papadimitroulas, Theodora Kostou, Konstantinos Chatzipapas, Dimitris Visvikis, Konstantinos A. Mountris, Vincent Jaouen, Konstantinos Katsanos, Athanasios Diamantopoulos, Dimitris Apostolopoulos, Athanasios Balomenos, Yiannis Kopsinis, George Loudos, Christos Alexakos, Dimitris Karnabatidis, and George C. Kagadis

***Abstract*—Pediatric patient-specific dosimetry of ionizing radiation is of great scientific and social interest. Children provide a higher relative cancer-risk from exposure to ionizing radiation compared to adults. The proposed study reviews the recent techniques applied in pediatric imaging and therapy applications for dosimetry purposes. Modern medicine makes use of advance computational tools for the personalization of internal and external dosimetry, especially in the sensitive group of children. Several groups of pediatric computational models have been developed which are combined with Monte Carlo (MC) simulations, machine learning (ML) techniques, and image processing algorithms for accurate dosimetry assessment. More specifically, this paper reviews the dosimetry applications in pediatric diagnostic procedures, including computed tomography and nuclear medicine applications. Right afterward, the most recent applications in therapeutic brachytherapy protocols are presented, which is a rather sensitive procedure in pediatrics. Finally, modern tools for dosimetry optimization are discussed, reviewing the most indicative applications with: 1) MC simulations for pediatric dosimetry assessment; 2) pediatric computational models, widely used in medical applications; and 3) ML techniques that provide an alternative method for estimating individualized absorbed doses.**

***Index Terms*—Monte Carlo (MC) simulations, pediatric computational models, personalized dosimetry.**

Manuscript received September 17, 2018; revised October 9, 2018; accepted October 12, 2018. Date of publication October 17, 2018; date of current version November 1, 2019. This work was supported by the European Union's Horizon 2020 Research and Innovation Programme through the Marie Skłodowska-Curie under Grant 691203. *(Corresponding author: George C. Kagadis.)*

P. Papadimitroulas is with Research and Development Department, Bioemission Technology Solutions, 11472 Athens, Greece (e-mail: panpap@bioemtech.com).

T. Kostou, K. Chatzipapas, and G. C. Kagadis are with the Department of Medical Physics, University of Patras, 26504 Rion, Greece (e-mail: theokost@upatras.gr; kwnchatz@upatras.gr; gkagad@gmail.com).

D. Visvikis is with INSERM UMR 1101, 29609 Brest, France (e-mail: dimitris.visvikis@inserm.fr).

K. A. Mountris and V. Jaouen are with LaTIM, University of Western Brittany, 29200 Brest, France (e-mail: konstantinos.mountris@gmail.com; vjaouen@gmail.com).

K. Katsanos and D. Karnabatidis are with the Department of Radiology, University of Patras, 26504 Rion, Greece (e-mail: katsanos@med.upatras.gr; karnaby@upatras.gr).

A. Diamantopoulos is with the Department of Interventional Radiology, Guy's and St. Thomas' NHS Foundation Trust London, London SE1 7EH, U.K. (e-mail: athanasios.diamantopoulos@gstt.nhs.uk).

D. Apostolopoulos is with the Department of Nuclear Medicine, University of Patras, 26504 Rion, Greece (e-mail: dimap@med.upatras.gr).

A. Balomenos and Y. Kopsinis are with the Department of Research and Innovation, LIBRA MLI, Edinburgh EH6 6JG, U.K. (e-mail: abalomenos@libramli.co.uk; kopsinis@ieee.org).

G. Loudos is with the Department of Biomedical Engineering, University of West Attica, 12210 Egaleo, Greece (e-mail: gloudos@teiath.gr).

C. Alexakos is with the Department of Industrial Information and Communication systems, ATHENA RC/Industrial Systems Institute, 26504 Rion, Greece (e-mail: alexakos@isi.gr).

Color versions of one or more of the figures in this paper are available online at http://ieeexplore.ieee.org.

Digital Object Identifier 10.1109/TRPMS.2018.2876562

I. Introduction

PATIENT specific dosimetry is of high interest in pediatric applications as radiation sensitivity is noteworthy higher compared to adults. Children have a higher risk of developing cancer compared to adults receiving the equivalent dose [1]. In addition, exposure to ionizing radiation in children has a longer period in which it may cause development of radiation-induced complications that may include cancer or as future parents, risk for passing on radiation-induced genetic defects in the next generations [2]. Diagnostic applications (CT/SPECT/PET), therapeutic schemes targeted radionuclide therapy and radiation treatment (RT) plans have to be reconsidered reflecting the individual characteristics of pediatric patients.

Radiation dose calculations from internal sources of radioactivity have been a challenge to our scientific society for over 50 years, from the simple thyroid self-dose estimates of Marinelli *et al.* [3] to the 3-D dose maps and dose-volume histograms for individual organs and tumors [4]. Over the past three decades, administered doses in pediatric nuclear medicine (NM) have evolved through clinical experience, considering the radiation-absorbed dose to the patient, the type of study required, available photon flux, instrumentation, and amount of time needed to perform the examination. Estimates of administered activities for children older than 1 year have typically been based on the recommended adult dose, corrected for body mass or body surface area [5], [6]. MIRD Pamphlet No. 17 [7] in 1999 presented the S-values at voxel level for the dosimetry of nonuniform activity distribution of radiation absorbed dose in body organs and tissues.

Previous studies have shown that increased exposure to medical radiation increases the incidence of cancer inductance [8], especially for those exposed in childhood or adolescence [9], [10] although the extent of the excess relative risk is still widely debated. The current methods to estimate organ and effective dose from medical imaging examinations

This work is licensed under a Creative Commons Attribution 4.0 License. For more information, see http://creativecommons.org/licenses/by/4.0/

are based on studies using physical or computational phantoms, and/or models [11]–[19]. Computer-based phantoms, with the flexibility to model an unlimited set of anatomies, have the greatest potential to estimate patient-specific organ and effective dose. Recent work in the development of computerized phantoms has focused on the creation of ideal "hybrid" models that seek to combine the realism of a voxelized phantom and the flexibility of a mathematical phantom. In addition, different morphometric categories include reference (limited database of phantoms by age at 50th height/weight percentile), patient-dependent (more extended database of phantoms covering a broad range of body shapes and sizes), patient-sculpted (phantoms altered to match the patient's unique outer body contour), and patient-specific (an exact representation of the patient with respect to both body contour and internal anatomy) [20].

The development of accurate anatomical virtual anthropomorphic models has reached a mature state for clinical exploitation [21]. Monte Carlo (MC) simulations are widely recognized as an essential method to study the physics of NM, radiology, radiation therapy, and dosimetry. Combined with accurate pediatric computational models, MC serve as reference for the accurate determination of absorbed dose, toward personalized dosimetry [22], [23]. The absorbed dose per organ is crucial for children, where significant organ differentiations exist compared to the adult population. The known anatomy of the models and the MC tracking of the particles serve as the ground truth in modern medicine.

Developing and optimizing dosimetry protocols in pediatric applications is therefore of great social interest and worldwide health community. However, there are important challenges to address.

1) The computational time and the need of computing resources for implementing heavy and accurate realistic MC simulations incorporating patient specific characteristics.
2) Validation of several clinical protocols used in pediatric diagnosis and therapy based on real data.
3) There are common difficulties on applying experimental dosimetry during clinical practice on children (such as the CT dosimetry-based TLDs at the surface of the body).

The aim of this review is to address the recent developments in pediatric computational models, MC simulations, machine learning (ML) techniques and advanced image processing algorithms for dosimetry applications. These advanced tools are required for the personalization of dosimetry assessment in pediatric applications and will offer the clinician the possibility to assess imaging and therapeutic protocols predicting the absorbed dose per organ with accuracy.

II. Dosimetry in Pediatric Diagnosis Applications

A. CT Dosimetry

Within the field of Radiology, X-ray imaging of the pediatric population for diagnosis and/or therapy routinely involves exposure to ionizing radiation for diagnostic and/or guidance purposes [24]. The Image Gently Alliance is a coalition of health care organizations dedicated to providing safe, high quality pediatric imaging worldwide [25], and its primary objective is to raise awareness in the imaging community of the need to adjust radiation dose when imaging children. The Image Gently campaign dictates certain general principles [26]. First, X-ray exposure should be considered/undertaken only when a clear diagnostic/medical benefit is expected. Second, radiation-free alternative imaging methods like ultrasonography and/or magnetic resonance imaging should be used if possible. Third, the safest imaging protocols and techniques matched to the size (not age) of the child must be practiced at all times.

Special attention should be paid in the optimization and modification of equipment, application of appropriate technique, and imaging parameters. Radiography represents 84% of all ionizing radiation imaging examinations in children. To best manage dose exposure while achieving good image quality for diagnosis, digital radiography (DR) (term used for both computed radiography and direct DR) is recommended over older generation analog screen-film technologies [26] because of its more than 100 times greater latitude of exposure and the versatility of digital image storage, distribution, and manipulation that may partly compensate for underexposure and overexposure of the relevant body [27].

The "Best practices in DR" white paper by the American Society of Radiology Technologists explores in detail the necessary steps and measures in the current era of DR [28]. In brief, prior to the medical examination, the radiographer should consult with the radiologist and/or ordering physician to ensure the clinical validity and appropriateness of the examination and prevent duplication. Departmental standards and protocols are usually centered around automatic exposure control (AEC), use of the highest kVp within the optimal range for the position and part coupled with the lowest amount of mAs needed to provide an adequate exposure to the image receptor, collimation of the X-ray beam to the anatomic area appropriate for the procedure, use of lead shielding for anatomic parts that are adjacent to the X-ray field, etc.

However, in pediatric radiology the effective radiation dose largely depends on patient thickness and target organ size and adult AEC settings are not recommended. X-ray absorption/transmission depends on the atomic number composition and thickness of the body part being imaged [29]. The Image Gently campaign recommends measuring the size of children with calipers if possible to ensure application of a standardized imaging technique [25]. The relevant size-generated technique charts may be used to appropriately size acquisition settings for each child [30].

Adult radiography employs anti-scatter grids to reduce scatter and improve contrast to noise ratio (CNR). Grids are infrequently used in pediatric DR according to both the American College of Radiology (ACR)—Society for Pediatric Radiology [31], and the ACR—American Association of Physicists in Medicine (AAPM)—society for imaging informatics [32] guidelines. Furthermore, care should be taken for appropriate positioning of the patient under the X-ray beam in combination with appropriate collimation prior to radiation

exposure. Collimation is necessary to protect body parts not contributing to the clinical diagnosis or image guidance.

With the aim to standardize exposure settings, and espoused by the 2004 ALARA conference in digital radiography [33], both the international electrotechnical commission (IEC) [34], and the AAPM, independently developed standardized terminology. There are three important terms to be learned by radiologists, radiologic technologists, and medical physicists according to the new IEC standard: target exposure index (EI_T), exposure index (EI), and deviation index (DI) [35]. EI is an index of the exposure of the detector in the relevant image region. EI_T is the target reference exposure when the image receptor is exposed properly. The DI measures how far the actual EI deviates from the theoretical EI_T and serves as an immediate feedback number to both the technologist and interpreting radiologist indicating the adequacy of the exposure [36]. Overall, use of exposure and deviation indices in routine everyday practice may standardize local quality improvement frameworks and help harmonize pediatric DR.

In the case of computed tomography (CT), it is estimated that more than 10% of the more than 100 million CT caseload per annum is performed in patients less than 18 years old [37]. Available risk estimates suggest that pediatric CT will result in significantly increased lifetime radiation and consequently cancer risk over adult CT examinations [38]. There are three aspects that are unique to radiation dose in CT. First, single axial CT images are acquired in a highly axial collimated manner; second, there is more homogeneous exposure of the tissue slice to radiation because of the rotational nature of the CT X-ray beam, and third, radiation dose to the slice volume is significantly higher because of the mAs and KVp settings used to achieve a higher signal to noise ratio and CNR. In addition, scattered dose in CT can be considerable and may be even higher than the radiation burden from exposure to the primary beam [39]. The CT dose index is defined as the integral of the dose profile along a line parallel to the axis of rotation for a single scan, divided by the nominal slice thickness and provides a good approximation of the average tissue dose from multiple scans. For pediatric CT protocols, the Image Gently campaign recommends development of children-specific CT protocols based on the thickness of the body part imaged, along with automatic tube current modulation, reduced KVp techniques and iterative reconstruction algorithms [40].

Frush *et al.* [41] have proposed the introduction of weight-based color-coded CT body protocols to optimize radiation exposure in children. These protocols employ fixed tube current and peak voltage according to the children's weight. Establishment of pediatric patient abdominal and pelvic diagnostic reference levels (DRLs) using AEC settings has also been recommended for all CT scanners in pediatric radiology departments and have already been developed in several European countries [37]. It has been shown that compliance with the aforementioned protocols and guidance may result in an up to 90% reduction of CT related radiation exposure [42]. In summary, for pediatric CT, dose reduction should be optimized by the adjustment of scan parameters according to patient weight or age, region scanned, and study indication (e.g., images with greater noise should be accepted if they are of sufficient diagnostic quality). Other strategies include restricting multiphase examination protocols, avoiding overlapping of scan regions, and only scanning the area in question. DRLs may help toward a quality assurance and improvement framework in pediatric CT [43].

Interventional radiology (IR) in children employs real-time fluoroscopy combined with digital angiography for the diagnosis and/or treatment of variety of medical conditions. Effective radiation dose estimates in IR may vary widely during pediatric IR procedures depending on the clinical aims at hand, the experience of the operator, the child's size and shape, and the challenges of the particular anatomy being investigated [44]. A certain level of training in radiological protection is desirable and—in some countries—mandatory to ensure optimal use of radiation [45]. Because of the dynamic nature of the IR procedures, maintaining the proper source to table/patient distance (no less than 15 In), minimizing patient to intensifier distance, and carefully adapting patient position and tight collimation around the area of interest along with minimization of fluoroscopy time with the least number of angiographic exposure runs are the key elements for a safe pediatric IR practice. In collaboration with the relevant vendors, children specific angiographic protocols may be installed, or custom made with dose reductions, variable frame rates and appropriate lengths of angiographic runs. Good medical practice within the IR angiography suite should also include routine use of "last image hold" and "fluoro save" options instead of proper runs, pulsed fluoroscopy with a rate as low as 3 pulses per second, and particular care not to expose the eyes, thyroid and gonads [46]. Finally, relevant exposure indices, including DAP, Air kerma, fluoroscopy time, etc., should be recorded and monitored as part of a regular quality assurance and improvement program [47].

In the conclusion, children have a longer life expectancy and therefore have a higher average risk of future cancer development compared to adults receiving the same dose of radiation. The importance of rigorous justification of the need for each radiological examination involving ionizing radiation cannot be over-emphasized, and the application of alternative radiation-free imaging modalities should always be considered. Imaging parameters may be adjusted, and protective measures may be instituted so that the required image is obtained with the lowest possible dose whilst sufficient image quality is maintained for diagnostic purposes or therapeutic guidance. Examples of good radiographic and fluoroscopic practice include attention to patient positioning, adequate collimation of field size, use of protective shielding as necessary, optimization of exposure factors, preferential use of pulsed over continuous fluoroscopy, CT tube current modulation and organ-based CT dose modulation along with auto kV technology and iterative reconstruction algorithms, etc. [1].

B. SPECT/PET Dosimetry

NM is a medical field involving the use of low radiation activities for diagnostic and therapeutic applications, appropriate for a big variety of clinical problems, such as different types of cancers, gastrointestinal, endocrine, neurological, and heart disorders. NM applications pinpoint the

spatial distribution of a radioactive pharmaceutical within the body, giving the opportunity for early disease diagnosis and therefore for improved patient's response to therapeutic operations [48]–[50].

Due to the small amounts of radiation exposure, the arising radiation risk from commonly used NM procedures is not significant and there is no evidence of unwanted health effects. Therefore, pediatric NM techniques are highly recommended. Nevertheless, it is important to consider the guidelines for justification and optimization of image quality, and dose [6], [51]. There is lack of documentation in the low-dose range of the long-term effects, while risk estimations below 100 mSv have big uncertainties [52]–[54].

Therefore, the methods leading to dose reduction are a matter of concern and can be achieved with plenty of ways, such as appropriate use, updated dose guidelines, adjusting imaging protocols, image processing, and the development of advanced imaging systems [55].

The appropriate use of a clinical application depends on physicians, who have to select the safest and most effective examination for a certain clinical problem and then have to optimize the performance of the exam. The choice of the most effective examination is a good strategy for early diagnosis, therefore facilitates the immediate beginning of the therapy, whereas, inadequate techniques can be harmful, increasing the total number of examinations and decreasing patient's comfort, cooperation and satisfaction.

Universal dose guidelines for administering radiopharmaceutical doses are essentials especially in pediatric applications. In 2008, a survey carried out in North America revealed that the administered doses of radiopharmaceuticals to children varied a lot, especially with respect to minimum total administered dose. This broad variation caused concerns and emphasized the urgent need to develop pediatric standards, according to the ALARA concept (as low as reasonably achievable) [5].

The Image Gently Alliance encouraged the collaboration of radiologic technologists, medical imaging physicists, and pediatric radiologists in order to achieve a standardization of the administered doses in pediatric NM. After the organization of four consensus workshops, the 2010 North American Consensus Guidelines for Pediatric Administered Radiopharmaceuticals were developed [56], [57]. Image Gently Alliance endorsed by the society of NM and molecular imaging (SNMMI) proposed these guidelines and additional posters and Web-based tools [58] have been developed.

The "A radiopharmaceuticals schedule for imaging in pediatrics" guidelines with formulas based on the body surface area and body-weight suggested minimum activities for mainly 99mTc-labeled radiopharmaceuticals were published by the Paediatric Task Group of the European Association of NM (EANM) [59]. Based on this paper, Jacobs *et al.* [60] proposed new cards to calculate weight-independent effective doses. Later EANM published a paediatric dosage card for 39 radiopharmaceuticals [61], and the dose limits for F-18 were updated with a new study in 2008 [62]. In addition, the EANM released an online dosage calculator [63] and generated an application for iPhone/iPad (iAPP) under a project of the European Union [64]. During 2012, the EANM and SNMMI collaborated to harmonize the guidelines proposed by the two associations [65], [66]. The publication of new of international guidelines (Pediatric Radiopharmaceutical Administration: Harmonization Guidelines), including twelve radiopharmaceuticals, was the result of this collaboration in 2014. Most of the weight-based administered activities were computed using adult reference activities, excluding gastric emptying and cystography. Special procedure guidelines for diuretic and standard renography in children were also addressed by SNMMI and the EANM [67], [68].

The differences of the suggested procedures between EANM (version 1.5.2008) and the 2010 North American Consensus Guidelines were reported on 2015. Standard models and nominal organ-weighting data were used to estimate critical-organ radiation doses for 5 typical pediatric patients and 12 diagnostic examinations. The 37% of the studied procedures had no remarkable difference, while in 24% of the cases, the resulting effective doses resulted from the American consensus guidelines were more than 20% higher, especially for dynamic renography (99mTc-MAG3) and 99mTc-sodium pertechnetate for radionuclide cystography [69]. In the rest of the cases (39%), the resulting effective doses resulted from the EANM were more than 20% higher. The basic difference occurs from the fact that weight-scaling is linear for the North American Consensus Guidelines and nonlinear for the EANM guidelines. The EANM pediatric dosage card was last updated and published in 2016 [70] and the North American guidelines published new recommendations for 12 more radiopharmaceutical applications [71]. The surveys that were followed showed that a few clinicians had followed the new guidelines [72], [73].

The Japanese society of NM (JSNM) guidelines are also widely used and have been translated into English. The JSNM Optimization Committee-based their results on a survey of 14 Japanese clinical centers. The proposed guidelines have the basis on the EANM class, baseline activity, and minimum activity, with weight-based normalization factors and 24 radiopharmaceuticals were modified. Fahey *et al.* [74] in 2016, reported the differences between the American Consensus Guidelines, the JSNM and the EANM dosage card. They concluded that all of them propose activities based on patient weight, but still have significant differences for some cases that should be further studied, especially for PET/CT minimum activities [75], [76].

Fine-tuning of the imaging protocols is also an efficient way to reduce the administered doses. The selection of the most effective type of examination, dynamic or static can optimize the radiation dose. For instance, some dynamic scintigraphies, such as ^{99m}Tc-MAG3 for renography and hepatobiliary scintigraphy are acquired by a first fast framing rate and then are followed by a slower framing [77].

The dose and the total time of the acquisition can also be reduced by advanced image processing algorithms, such as the application of spatially adaptive filtering software [78], [79]. Adapting the degree of filtration to the image, random noise can be decreased, keeping the spatial resolution high. Iterative

image reconstruction provides high-quality studies, obtained with much lower radiation exposure to the patient and shorter acquisition times [80]–[84].

Improvements of the conventional instrumentation in NM, such as optimized collimators for SPECT can increase the sensitivity of a study and therefore reduce radiation burden [85]. In addition, solid-angle coverage in SPECT and PET can also help to detect many more counts at a time, and detector advances in new materials and technologies can also contribute to a reduction of administered dose in pediatrics [86].

A new dosimetry methodology was proposed recently, within the ERROR project [87], for personalizing the assessment of pediatric dosimetry, considering the anatomical differences of pediatric patients. The specific absorbed dose rates metric was introduced and validated both in preclinical and pediatric applications, creating new dosimetry databases [88], [89].

III. Brachytherapy Dosimetry in Pediatric Therapy Applications

Brachytherapy (BT) is a widely used alternative treatment option to external beam radiotherapy (EBRT) for the confrontation of various cancer types in adults (e.g., prostate, breast, cervical, gynecological, etc.). Advantages of BT over EBRT are namely the high radiation conformity to the target area; the high local control rate (80%) [90]; and the reduced dose delivery to surrounding healthy tissue.

In face of the referred advantages, BT has become an important aspect in the treatment of pediatric malignancies. Pediatric patients (age <21) cannot be considered small adults. Tumors in these patients are generally very sensitive to both chemotherapy and radiotherapy, and long-term toxicities (e.g., growth retardation) are of great importance. The potential danger of adverse effects of ionizing radiation upon growth and normal tissue development, as well as potential second malignancy induction restricts the delivery of high radiation dose [91]. The ability to deliver localized dose with increased dose sparing of healthy proximal tissue renders BT a valuable asset for the cancer treatment of pediatric population. BT can be used as standalone therapy or more commonly in combination with surgical resection. Patients with large tumor bed cannot be treated with BT alone and require low-dose EBRT boost when surgical resection is not performed [92].

We have reviewed the available literature from 1994 to 2018 and we noticed a considerable increase of BT application for the treatment of pediatric carcinomas. Clinical trials reporting the local control (LC), overall survival (OS), morbidity, toxicity, and side-effects have been performed investigating the effectiveness of various BT types [93]–[101]. Low dose rate BT (LDR-BT), intraoperative high dose rate BT (IO-HDR-BT), and pulsed dose rate BT are few of the considered BT types in the so far clinical experience with BT.

Clinical Experience With BT in Pediatrics: The largest clinical experience with BT in pediatrics has been reported for soft-tissue sarcoma [94], [97], [99], [100]. Furthermore, clinical trials on patients with solid tumors [95], low-grade gliomas [96], [101], and genital cancer—for both male [93] and female [98] pediatric populations—have been published. Merchant *et al.* [99] have reported on the treatment of soft-tissue sarcoma with BT alone or as boost to EBRT. A population of 31 patients that received treatment between 1988 and 1999 at St. Jude Children's Research Hospital was considered. Patients were treated with temporary or permanent interstitial implants using iridium-192 or iodine-125. No local or regional failures were recorded in the group treated with BRT alone ($n = 10$). On the other hand, when BT and EBRT were combined ($n = 21$) there were one local failure, two regional failures, and three patients who developed pulmonary metastasis. The median survival was 34 months. The most common reported BT-related side effects were wound dehiscence, fibrosis/telangectasia, pigment changes, and cellulitis. Patients received 900–1000 cGy per day to a minimum 5 mm tissue depth.

Nag *et al.* [100] have studied the effectiveness of IO-HDR-BT for the treatment of soft-tissue sarcoma patients. From 1992 through 1999, 13 pediatric patients were treated with a combination of chemotherapy, EBRT, IO-HDR-BT, and surgical resection. The dose delivered at 5 mm tissue depth with IO-HDR-BT was 10–15 Gy. EBRT dose was restricted to 27–30 Gy. The median follow-up was 47 months (range 12–97). OS was 85% (11 patients alive). The reported LC rate was 95% and the distant failure rate 23%. The authors concluded that IO-HDR-BT is most effective when used as boost of 10–20 Gy in completely resected or minimally residual tumors. The dosimetric advantage of IO-HDR-BT in treating superficial residual tumors and previously irradiated fields while avoiding underlying critical structures has been reported.

More recently, Folkert *et al.* [94] performed a larger retrospective study (75 patients) reporting on their 20-year experience (1993–2013) with IO-HDR-BT for pediatric sarcoma treatment. The median follow-up was 7.8 years. The 5-year rates of LC, OS, and event-free survival were 63% (50%–76%), 43% (30%–55%), and 33% (21%–45%). Acute toxicity $\geq$ grade 3 and late toxicity $\geq$ grade 3 occurrence were found 2.5% and 5.3%, respectively, at 0.3–9.9 years after IO-HDR-BT. All toxicity $\geq$grade 3 occurred in patients ≤ 6 years treated with IO-HDR-BT doses $\geq$ 12 Gy. Therefore, it was concluded that doses between 8–12 Gy are appropriate for IO-HDR-BT in patients ≤ 6 years of age.

Similarly, Laskar *et al.* [97] reported high LC in a clinical study, including 105 children with soft-tissue sarcoma who were treated with BT from 1984 through 2014. Median follow-up was 65 months. LC and OS at 10 years were found 83 and 73%, respectively. Tumor size and location were found significant while there was not considerable difference in LC between patients receiving BT alone or BT combined with EBRT (84% versus 80%, $P = 0.43$). Negligible difference in LC was also reported between LDR-BT and IO-HDR-BT (86% versus 83%, $P = 0.30$). From the 105 patients, 33 (31%) received LDR-BT and 72 (69%) IO-HDR-BT. Combination of BT and EBRT was delivered to 20 patients with median EBRT dose 45 Gy (range: 30–60 Gy, 1.8–2 Gy daily fractions) and LDR-BT dose 25–30 Gy (median: 30 Gy). IO-HDR-BT dose was 15 Gy in five fractions. For the patients treated with BT alone, median LDR-BT dose was 39.5 Gy (range: 35–50 Gy)

and median IO-HDR-BT dose was 36 Gy in nine fractions (range: 24.5–40 Gy, 3.5–4 Gy fraction, over 6–10 fractions).

Clinical experience with IO-HDR-BT has also been reported for solid tumors [95]. In this paper, Goodman *et al.* analyzed retrospectively records of 66 patients for a period of 10 years (1993–2002). LC and OS actuarial rates after 2 years were reported 56% and 54%, respectively, with a median survival of 29 months. In cases, where EBRT was also delivered the 2-year LC significantly improved (83% versus 29%). The actuarial 2-year late complication rate was 12%. Late local complication events were limited to 12% and included small bowel obstruction, broncho-esophageal fistula, and bone growth retardation. Based on these findings, the authors concluded that IO-HDR-BT has a potential benefit when combined with EBRT for pediatric patients with solid tumors.

Considering children with low grade gliomas (LGGs), stereotactic BT (SBT) with iodine-125 has been proven a highly effective local treatment option for pediatric patients with unresectable or residual LGG WHO grades I and II. Ruge *et al.* [101] have reported survival rates at 5 and 10 years at 93% and 82%, respectively. From the 147 included patients, 21 (14.8%) presented tumor relapse. For the remaining patients, 24.6% revealed completed response, 31.0% partial response, and 29.6% stable disease. The considered patients were treated with 50–65 Gy cumulative therapeutic dose delivered within 9 months. Kunz *et al.* [96] reported similar results in a clinical study performed on 58 pediatric patients. SBT alone was performed on patients with LGG of $\leq$ 4 cm in diameter. For larger tumors, best safe resection was combined with SBT. The median delivered dose was 54 Gy. Five-year survival was reported 87%. Moreover, the overall early (delayed) toxicity rate was 8.6% (10.3%), respectively, and no permanent morbidity has occurred.

Pediatric BT Dose Guidelines: Dose guidelines in BT for pediatric patients depends strongly on factors, such as patient's age, tumor's type, tumor's radiosensitivity and selected BT type. According to the considered literature additional clinical trials are deemed necessary to conclude on dose recommendations.

Soft-Tissue Sarcoma: For temporary or permanent implants with iridium-192 or iodine-125, 900–1000 cGy per day to a minimum 5 mm tissue depth are recommended. For IO-HDR-BT, 10–15 Gy delivered dose at 5 mm tissue depth is recommended. If combined with EBRT, the EBRT dose should be restricted to 27–30 Gy. IO-HDR-BT may be more effective as boost of 10–20 Gy in completely resected or minimally residual tumors. When patients $\leq$ 6 years of age, then 8–12 Gy are appropriate for IO-HDR-BT. Higher doses increase the chance for toxicity $\geq$ grade 3 in this group.

Solid Tumors: For treatment areas ranging from 6 to 345 cm^2 implants with iridium-192, the prescribed dose to 5 mm tissue depth ranges from 4–15 Gy.

Low Grade Glioma: When lower grade glioma WHO type I or II is treated with SBT using iodine-125 implants, a cumulative therapeutic dose of 50–65 Gy delivered within 9 months is proven highly effective for patients with unresectable or residual tumors.

IV. Modern Tools for Dosimetry Optimization

A. MC Simulations

MC mathematical techniques can be described as statistical methods that use random generators to perform realistic simulations for specific cases. MC simulations simplify the calculations that best describe the physical (and recently chemical) interactions that are taking place in an application (e.g., production of secondary charged particles, very-low energy photon interactions, electron ionization, photon elastic scattering, attenuated particles, etc.). Over the last years, computer science has been vigorously evolved, speeding up MC simulations by enabling graphical physical units (GPUs), as well as clusters and grids of central processing units (CPUs) and high-performance computers (HPCs).

Several MC codes have been exploited (Table I). We can refer EGS [102], ITS [103], MCNP [104], ETRAN [105], PENELOPE [106], [107] and Geant4 [108]. Geant4 [109] managed to be one of the leading reference MC codes in the field of medical physics, for clinical and preclinical simulations. This statement can be understandable by the future widely used MC codes that were developed based on the core of Geant4. GATE [110], GGEMS [111], GAMOS [112], TOPAS [113], and PTSIM [114], are typical examples of such codes. GATE is an advanced toolkit developed by the international OpenGATE collaboration [115] and is dedicated to numerical simulations in medical imaging and radiotherapy (PET, SPECT, CT, RT, Dosimetry). GGEMS [116] is an advanced platform using GPU architecture targeting medical applications (imaging and particle therapy).

Studies referring to pediatric dosimetry using MC simulations have been increased over the past years. They evaluate CT as while as NM imaging protocols. Straton *et al.* [117] and Lee *et al.* [118] used MCNP5 to simulate the irradiation of newborn patients by a 16 helical scanner. A new approach in which patient size and not only age was used to correlate dose with the risk was investigated by Li *et al.* [119] and they also widen their study to 42 different patient models [120] they used an upgraded version of PENELOPE. Studies have also been done for the dosimetric evaluation of CT protocols used for pregnant patient and the fetus [121]. Another technique used for dose-saving is tube current modulation. Schlattl *et al.* [122] used EGS to evaluate its impact on the dose when used on pediatric patients. One more study focused on dose calculations for 40 pediatric patients using Geant4 [123]. Currently, the ERROR dosimetry software [87], based on GATE, aims to optimize dosimetry during pediatric CT examinations by modeling and validating clinical commercial CT scanners. The process of simulating a CT protocol with GATE software is summarized in Fig. 1. The proposed methodology is to create a simulated dosimetry database using a large population of several pediatric models. Thus, the database could be used in clinical practice by matching every new patient to the closest anatomical pediatric model and to extract the precalculated absorbed doses per organ for the specific imaging protocol and for the specific CT scanner [48], [49].

MC simulation techniques appear the most precise and advanced approach for internal dose calculations [124]–[126].

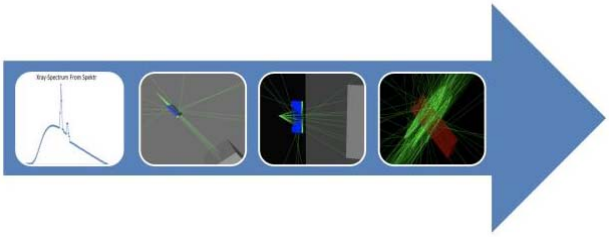

Fig. 1. Process in MC software for the CT simulation. (a) Generation of spectrum. (b) Geometry definition (focal spot, fan and cone angles). (c) Filtration definition (bowtie filter). (d) Source Path definition (collimation, pitch, start and stop locations).

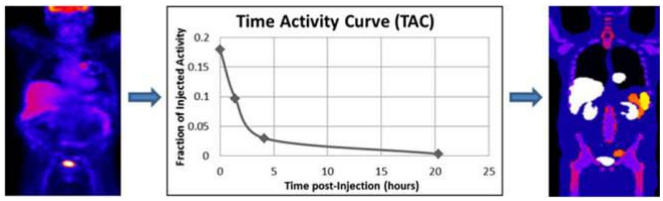

Fig. 2. Simulation procedure in GATE for an NM study. Manual region of interest segmentation is applied to the clinical data to derive the time activity curves of the organs of interest. The resulting whole-body activity biodistribution is inserted into the phantoms and used for voxel-based radiation transport and dose deposition simulations integrated over time.

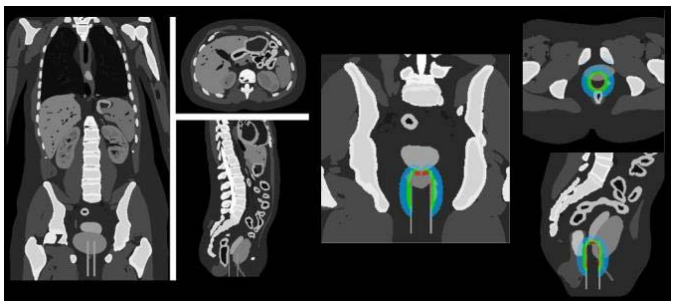

Fig. 3. Simulation of a pediatric BT application. Isodose curves are depicted.

These techniques are also getting into the clinical practice with the development of more user-friendly software, such as the Minerva, Celldose, RADAR, DOSIMG, 3D-RD, OEDIPE and DPM [127]–[133]. For research purpose different teams have different code for dosimetry of NM, such as the MCNP [134]–[137], FLUKA [138], and Geant4 [139], [140]. At last, GATE MC code [22] has been widely used for internal dosimetry [89], [141]–[147]. Fig. 2 shows the procedure for the simulation of an NM study in GATE.

There is also a radiotherapy study comparing MC techniques with a clinical Treatment Planning System, for Proton therapy dose distribution to pediatric patients [148]. In another radiotherapy study, several commercial BT seeds were modeled and validated which could be directly applied in MC treatment simulations for pediatric purposes. Initial results were presented by Chatzipapas *et al.* [149].

Fig. 3 presents the phantom used for the BT simulation and the corresponding isodose curves that were depicted.

TABLE I
MAIN MC CODES CATEGORIZED IN "GENERIC" AND "DEDICATED," INCLUDING THEIR MAIN CHARACTERISTICS

Name	Description
Generic codes	
EGS4	SLAC (US), the National Research Council of Canada and KEK (Japan)
ITS	Sandia National Laboratories, (US)
MCNP	Los Alamos National Laboratory (US)
GEANT4	CERN (EU)
PENELOPE	University of Barcelona (EU)
ETRAN	Center for Radiation Research (US)
Dedicated codes	
PTSIM	Particle Therapy – RT – Dosimetry (based on Geant4)
FLUKA	Dosimetry
TOPAS	Particle Therapy – RT – Dosimetry (based on Geant4)
GAMOS	SPECT – PET – RT – Dosimetry (based on Geant4)
GGEMS	Dosimetry – GPU capabilities (based on Geant4)
GATE	SPECT – PET – RT – Dosimetry (based on Geant4)
Dedicated software for NM	
Minerva	Based on Peregrine
Celldose	Based on EGS4
RADAR	Based on EGS4
DOSIMG	Based on EGS4
3D-RD	Based on EGS
OEDIPE	Based on MCNPX
DPM	

B. Pediatric Computational Phantoms

Committee II of the ICRP was given the task of developing recommended limits for the maximum permissible amounts of radionuclides that could be delivered to the human body [150]. The committee modeled the human body as a set of separate spheres, whose size and composition were based on the characteristics of the "standard man." The current generation of anthropomorphic phantoms began with the development of the Fisher–Snyder phantom [151]. This phantom used a combination of geometric shapes to create a more anatomically accurate representation of the body. This phantom was used with MC techniques, which simulated the creation and transport of photons through these various structures in the body whose atomic composition and density were based on data provided in the ICRP report on the Reference Man [152]. The MIRD method [153] for internal dosimetry has been used for many years, employing S values in combination with agent-specific biokinetic data, to obtain organ doses for various radionuclides. Dose estimates thus derived, are applicable only to an individual who is well represented by the size and shape of the Reference Man. Even then, there may be

considerable differences between the real structures of the body and the stylized representations of it in the computerized phantom. Nonetheless, this has been the state of the art for two decades and is still widely used in internal dose assessment. The development of the Cristy and Eckerman [154] phantoms allowed dose calculations for different individuals, for variable size and age. Six phantoms were developed, which were assumed to represent children and adults of both genders. Absorbed fractions for photons at discrete energies were published for these phantoms, which contained approximately 25 source and target regions. The *S* value datasets were made available in the MIRDOSE computer software [155]. Lee *et al.* [156] proposed six more computational phantoms of pediatric patients. They are tomographic computational phantoms which provide distinct advantages over stylized phantoms, such as the MIRD. The UF hybrid reference phantoms [157] are well suited for manual adjustment to match anthropometry. Researchers have developed methods to systematically scale phantoms to various body morphometries using the software Rhinoceros.

The handbook of Anatomical Models for Radiation Dosimetry has been published reviewing the whole history and progress of anatomical computational models [21]. Xu *et al.* [158] proposed a different approach than MIRD, leading to an image-based whole-body adult male model, constructed using color photographs, the VIP-Man. DUKE University has developed a series of realistic 4-D anthropomorphic models (XCAT model [159]) based on the nonuniform rational b-spline (NURBS) and subdivision surfaces. In 2009, the ITIS foundation developed and published the "virtual family"; a series of surface-based anatomical models, including two children. Two years later they extended their dataset with a "virtual classroom," including four more children based on healthy clinical MR data [160].

Recently some realistic phantoms have been published [161]. In this paper, 80 deformable pediatric reference NURBS computational phantoms are described, ranging from newborn to 15-year-old, male and female. They follow the guidelines for reference anatomies and organ masses of normal-stature children.

Another work contains the largest library available today, including 1100 female and male pediatric phantoms [162]. The population contains newborn, 1, 2, 5, 10, and 15-year-old children. The computational phantoms were evaluated with qualitative approach using 3-D visualization as while as quantitatively by the analysis of internal organ masses. They follow the same trend as the ICRP reference data, when correlated with age.

A series of in-house pediatric models are also developed using clinical whole-body PET/CT data within the ERROR dosimetry software. At least ten pediatric patients are converted in computational models with different anatomical characteristics and varying in gender, age, mass, height [163].

C. Machine Learning Techniques

Accurate organ segmentation is a vital step in dosimetry since it affects the computed organ volumes, shapes and relative positions. Manual segmentation of 3-D medical images is highly labor intensive rendering it impractical especial when it concerns the full body, multiorgan segmentation scenario, which is the case for the creation of computational phantoms. Organ and tissue segmentation can be cast as a pixel-wise classification task and as such a wide range of ML algorithms and techniques are applicable either directly or as ingredients in the segmentation pipeline [164].

Until recently, Atlas guided methods [163], [165] were the most powerful approaches when attempting automatic multiple organ segmentation. These methods naturally incorporate spatial information, information on anatomy, shape, size, and features of different, organs or soft tissues in the form of anatomical atlases [166]–[173] or statistical shape models [169], [174], [175] which are calculated by averaging location or shape priors of multiple spatially aligned atlases. In principle, atlas-based methods rely on the pairwise intersubject registration of the medical image that need to be segmented to one or more predefined deterministic or probabilistic anatomical atlases in order to convey *a-priori* information associated to the position and/or shape of the organs of interest facilitating the segmentation process. However, medical image registration process is a challenging task since most of the organs relative positions and appearance, especially the abdominal ones, vary considerably between patients due to natural variability, medical treatments, and soft tissue deformation [176]. ML has been recently employed to better assist and enhance the atlas selection and the registration process in atlas-based segmentation approaches [168], [171] leading to some improvements.

The recent advances in deep learning have rendered deep convolutional neural networks (CNNs) the methodology of choice in numerous classification tasks and applications [177]. The same is true in medical imaging in general and organ segmentation specifically [178]. These methods, in general, offer registration free segmentation with performance better than conventional atlas-based registration. The landmark year for the introduction of deep learning to the field is 2016 with a deluge of research works employing breakthroughs recently emerged in computer vision and semantic segmentation [179], [180] adjusted in higher or lessen degree to the peculiarities of the medical image organ segmentation setup. The most critical CNN variants which at the moment offer clear performance advantages are those operating in a fully convolutional end-to-end fashion employing directly the 3-D volumes generated in CT imaging. In their basic setup, these deep neural networks (DNNs) usually equipped with skip connections in a U-Net topology, are directly fed with the entire CT scan or relatively large subvolumes of it (rather than a densely patched version of it and/or operating in 2-D slice-by-slice fashion) providing a direct full resolution segmentation map of the organs under consideration [181]–[183].

The aforementioned 3-D DNN approaches suffer from a major drawback, which poses certain challenges to their application; they are extremely memory hungry a problem that tends to be more intense when the multiorgan case is considered. A number of rather ad-hoc practices, such as reducing the network depth, working on down-sampled versions of the CT

image or working on small patches of the CT image have been considered hampering, though, the segmentation performance. More sophisticated alternatives, which are explicitly trying to tackle the complexity of 3-D CNNs and higher memory requirement problem have also appeared, e.g., using 3-D representations with fewer, but higher-resolution, features by using dense blocks [184]–[186] or working with 2-D multiview aspects of the data and 3-D majority voting in a compact all-in-one network fashion [187].

With respect to training data requirements, the research studies above used from 90 to more than 300 properly annotated CT scans. This figure is large, comparable, however, to the number of atlases required in atlas-based approaches.

Many of the CNN approaches above have been recently incorporated in the TensorFlow-based open-source CNNs platform, NiftyNet [188] facilitating research in medical image analysis and image-guided therapy.

Multiple organ segmentation in pediatric medical imaging poses extra difficulties, which have not yet investigated under the novel deep learning technologies perspective. Indeed, CNN-based segmentation, so far mostly concerns adult populations. A major with pediatric CT-scan segmentation is that tends to be noisier and less detailed compared to adult scans due to the low dose acquisition protocols that are used. Furthermore, children usually move during the acquisition resulting in artifacts and blurry images. Moreover, pediatric CT-scans exhibit a much larger variability across kid ages. For the reasons above, it is an open issue to study the performance as well as the adequate number of training data required in the pediatric case.

CNN-based segmentation has already been explicitly used in the segmentation stage preceding organ-specific radiation dose calculation, e.g., for treatment planning in radiation oncology [189]–[193]. These works are focusing on a single organ or a small set of organs at risk (e.g., lungs, spinal cord, esophagus, and heart). Fu *et al.* [194] is the first 3-D CNN-based organ segmentation concerning an extensive range of 14 organs, which is explicitly used as preprocessing stage for dose estimation via MC simulations. In this method, the CNN segmentation model was combined with an alternative approach in order to deal with organs hard to be segmented. The latter were filled up by the corresponding organs of appropriately selected and transformed XCAT phantoms. The overall approach showed remarkably close dose calculations with those computed based on manual segmentation (2% difference for the segmented organs). An alternative path followed in [195], where a 22-layer CNN used for the detection rather than the exact segmentation of 16 different organs from the axial view of CT images. This allowed the classified organs to be automatically mapped to the slab number of a mathematical phantom to determine the scan range of ImPACT CT dose calculator.

Both methods above require the patient CT scan to be taken for the organ-specific dose calculation to take place, so they are useful for the effective generation of new computational phantoms or for hospitals to keep a record of dose per patient CT scan to monitor and manage radiation risks. They are not directly useful, however, for the prediction and assessment of the dose per organ that will be absorbed from a certain medical procedure before the latter takes places something that of critical interest especially in the pediatric case. The major established approach which succeeds in organ dose estimates prior to the medical exam is the convolution-based radiation field estimation approach developed at Duke University, which concerns tube current modulated CT [196]. According to this approach a new clinical patient is matched to a unique member of a library of computational phantoms according to a single anthropometric characteristic, namely the trunk height, defined as the distance between the top of clavicle to the end of pelvic region. Such a patient matching provides information about the patient's z-dimensional organ distribution prior to the CT examination, which is used to quantify regional irradiation field corresponding to specific organs. The impact of the body size and shape was accommodated exploiting the average chest and abdominopelvic diameter in order to normalize organ dose guided by an exponential regression model. Recently, GE Healthcare announced that has licensed a CT organ dosimetry technology that is based on the above principles [197].

V. Conclusion

In this paper, a review on the evolvement of pediatric dosimetry has been applied, referring the medical protocols used in clinical practice. A large number of medical societies and agencies are working together toward the promotion of radiation protection for children through updated guidelines, good strategies, improved instrumentation, and reconstruction algorithms. The rapid evolution of computer technology in combination with the clinical needs of modern medicine for personalized protocols, have emerged the growth of numerous pediatric models, fast simulation procedures (GPU, HPC, etc.) and new deep learning techniques that can predict dosimetry using large databases of presimulated data. The individual anatomical and functional characteristics play crucial role in the assessment of accurate dosimetry and modern medicine and the scientific community aim to overcome obstacles for such an issue of pediatric dosimetry.

The recent published research studies in the last decays have shown the potentiality of reconsidering the dosimetry that is currently applied in clinical routine, toward to personalized protocols. The "hybrid" computational patient-specific phantoms are considered to be the best representation in terms of physiological and functional information of the human body at the organ and cellular levels [198]. In a more recent study, Xie *et al.* [162], also concluded that a hybrid anthropometric paediatric phantom library for internal radiation dosimetry represents an efficient and flexible way to describe realistically the anatomy of the human body and offer unique advantages for patient-specific absorbed dose assessment and individual risks estimations. The advantage of patient-specific phantoms in comparison with patient-dependent hybrid phantoms, in its ability to predict patient dose with accuracy was also addressed Marshall *et al.* [199] for pediatric patients undergoing fluoroscopically guided cardiac procedures. Moreover, Stepusin *et al.* [200] concluded that matching a patient to

a computational hybrid phantom in a library is superior to matching to a reference phantom.

In the next few years, we anticipate that developments in the hybrid phantom technology will further evolve and will significantly improve organ dose assessments in several clinical applications. Functionalized, dynamic computational phantoms with more detailed nerve trajectories, lung and heart motion, vascular blood flow and thermal properties will be rapidly developed [201]–[203]. Moreover, cellular and even DNA-level models combined with MC simulations have been used to deeply comprehend the effects of radiation dosimetry [204]–[206]. The trend in modern medicine gives a positive insight for the achievement of personalized dosimetry during diagnostic and therapeutic medical procedures by correlating the absorbed dose to critical organs with biological, thermal, and genetic effects. Important findings in the fields of computer science, engineering, and biology will offer a boost in the understanding of radiation in medicine.

ACKNOWLEDGMENT

The results published in this paper reflect only the author's view and the Research Executive Agency and the European Commission is not responsible for any use that may be made of the information it contains.

REFERENCES

[1] P. L. Khong *et al.*, "ICRP publication 121: Radiological protection in paediatric diagnostic and interventional radiology," *Ann. ICRP*, vol. 42, no. 2, pp. 1–63, Apr. 2013.

[2] G. Alzen and G. Benz-Bohm, "Radiation protection in pediatric radiology," *Dtsch Arztebl Int.*, vol. 108, no. 24, pp. 407–414, Jun. 2011.

[3] L. D. Marinelli, E. H. Quimby, and G. J. Hine, "Dosage determination with radioactive isotopes; practical considerations in therapy and protection," *Amer. J. Roentgenol. Radium Therapy*, vol. 59, no. 2, pp. 260–281, Feb. 1948.

[4] R. K. Bodey, G. D. Flux, and P. M. Evans, "Combining dosimetry for targeted radionuclide and external beam therapies using the biologically effective dose," *Cancer Biotherapy Radiopharmaceuticals*, vol. 18, no. 1, pp. 89–97, Feb. 2003.

[5] S. T. Treves, R. T. Davis, and F. H. Fahey, "Administered radiopharmaceutical doses in children: A survey of 13 pediatric hospitals in North America," *J. Nucl. Med.*, vol. 49, no. 6, pp. 1024–1027, Jun. 2008.

[6] F. H. Fahey, S. T. Treves, and S. J. Adelstein, "Minimizing and communicating radiation risk in pediatric nuclear medicine," *J. Nucl. Med.*, vol. 52, no. 8, pp. 1240–1251, Aug. 2011.

[7] W. E. Bolch *et al.*, "MIRD pamphlet No. 17: The dosimetry of nonuniform activity distributions–radionuclide S values at the voxel level. Medical internal radiation dose committee," *J. Nucl. Med.*, vol. 40, no. 1, pp. 11S–36S, Jan. 1999.

[8] National Research Council, *Health Risks From Exposure to Low Levels of Ionizing Radiation BEIR VII Phase 2*. Washington, DC, USA: Nat. Res Council, 2006.

[9] D. Brenner, C. Elliston, E. Hall, and W. Berdon, "Estimated risks of radiation-induced fatal cancer from pediatric CT," *AJR Amer. J. Roentgenol.*, vol. 176, no. 2, pp. 289–296, Feb. 2001.

[10] J. D. Mathews *et al.*, "Cancer risk in 680,000 people exposed to computed tomography scans in childhood or adolescence: Data linkage study of 11 million Australians," *BMJ J.*, vol. 346, May 2013, Art. no. f2360.

[11] M. Caon, G. Bibbo, and J. Pattison, "Monte Carlo calculated effective dose to teenage girls from computed tomography examinations," *Radiat. Protect. Dosimetry*, vol. 90, no. 4, pp. 445–448, 2000.

[12] C. L. Chapple, S. Willis, and J. Frame, "Effective dose in paediatric computed tomography," *Phys. Med. Biol.*, vol. 47, no. 1, pp. 107–115, Jan. 2002.

[13] J. J. DeMarco *et al.*, "Estimating radiation doses from multidetector CT using Monte Carlo simulations: Effects of different size voxelized patient models on magnitudes of organ and effective dose," *Phys. Med. Biol.*, vol. 52, no. 9, pp. 2583–2597, May 2007.

[14] B. He *et al.*, "Evaluation of quantitative imaging methods for organ activity and residence time estimation using a population of phantoms having realistic variations in anatomy and uptake," *Med. Phys.*, vol. 36, no. 2, pp. 612–619, Feb. 2009.

[15] W. Huda and K. M. Ogden, "Computing effective doses to pediatric patients undergoing body CT examinations," *Pediatr. Radiol.*, vol. 38, no. 4, pp. 415–423, Apr. 2008.

[16] W. S. Snyder, *MIRD Pamphlet #11: S, Absorbed Dose Per Unit Cumulated Activity for Selected Radionuclides and Organs*. Reston, VA, USA: Soc. Nucl. Med., 1975.

[17] M. G. Stabin, "MIRDOSE: Personal computer software for internal dose assessment in nuclear medicine," *J. Nucl. Med.*, vol. 37, no. 3, pp. 538–546, Mar. 1996.

[18] M. Zankl, W. Panzer, H. Petoussi-Henss, and G. Drexler, "Organ doses for children from computed tomographic examinations," *Radiat. Protect. Dosimetry*, vol. 57, nos. 1–4, pp. 393–396, 1995.

[19] M. Cristy, *Mathematical Phantoms Representing Children of Various Ages for Use in Estimates of Internal Dose*. Oak Ridge, TN, USA: Oak Ridge Nat. Lab., 1980.

[20] C. Lee *et al.*, "Hybrid computational phantoms of the male and female newborn patient: NURBS-based whole-body models," *Phys. Med. Biol.*, vol. 52, no. 12, pp. 3309–3333, Jun. 2007.

[21] X. G. Xu and K. F. Eckerman, *Handbook of Anatomical Models for Radiation Dosimetry*. Boca Raton, FL, USA: CRC Press, 2009.

[22] D. Sarrut *et al.*, "A review of the use and potential of the GATE Monte Carlo simulation code for radiation therapy and dosimetry applications," *Med. Phys.*, vol. 41, no. 6, Jun. 2014, Art. no. 064301.

[23] J. Seco and F. Verhaegen, *Monte Carlo Techniques in Radiation Therapy*. Boca Raton, FL, USA: CRC Press, 2016.

[24] M. S. Linet, K. P. Kim, and P. Rajaraman, "Children's exposure to diagnostic medical radiation and cancer risk: Epidemiologic and dosimetric considerations," *Pediatr. Radiol.*, vol. 39, no. S1, pp. S4–S26, Feb. 2009.

[25] S. Don *et al.*, "Image gently campaign back to basics initiative: Ten steps to help manage radiation dose in pediatric digital radiography," *AJR Amer. J. Roentgenol.*, vol. 200, no. 5, pp. W431–W436, May 2013.

[26] M. J. Goske *et al.*, "The 'image gently' campaign: Increasing CT radiation dose awareness through a national education and awareness program," *Pediatr. Radiol.*, vol. 38, no. 3, pp. 265–269, Mar. 2008.

[27] C. E. Willis, "Computed radiography: A higher dose?" *Pediatr. Radiol.*, vol. 32, no. 10, pp. 745–750, Oct. 2002.

[28] T. L. Herrmann *et al.*, "Best practices in digital radiography," *Radiol. Technol.*, vol. 84, no. 1, pp. 83–89, 2012.

[29] P. L. Kleinman, K. J. Strauss, D. Zurakowski, K. S. Buckley, and G. A. Taylor, "Patient size measured on CT images as a function of age at a tertiary care children's hospital," *AJR Amer. J. Roentgenol.*, vol. 194, no. 6, pp. 1611–1619, Jun. 2010.

[30] S. P. Knight, "A paediatric X-ray exposure chart," *J. Med. Radiat. Sci.*, vol. 61, no. 3, pp. 191–201, Sep. 2014.

[31] American College of Radiology. (Aug. 8, 2018). *ACR-SPR Practice Guideline for General Radiography*. [Online]. Available: http://www.acr.org/Quality-Safety/Standards-Guidelines/~/media/ACR/Documents/PGTS/guidelines/General_Radiography.pdf

[32] American College of Radiology. (Aug. 8, 2018). *ACR-SIIM Practice Guideline for Digital Radiography*. [Online]. Available: http://www.acr.org/~/media/3E08C87AD6E6498D9E19769E5E5E390D.pdf

[33] C. E. Willis and T. L. Slovis, "The ALARA concept in pediatric CR and DR: Dose reduction in pediatric radiographic exams—A white paper conference executive summary," *Pediatr. Radiol.*, vol. 34, no. S3, pp. S162–S164, Oct. 2004.

[34] *Medical Electrical Equipment: Exposure Index of Digital X-Ray Imaging Systems. Part 1. Definitions and Requirements for General Radiography*, IEC Standard 62494-1, 2008.

[35] J. A. Seibert and R. L. Morin, "The standardized exposure index for digital radiography: An opportunity for optimization of radiation dose to the pediatric population," *Pediatr. Radiol.*, vol. 41, no. 5, pp. 573–581, May 2011.

[36] S. J. Shepard *et al.*, "An exposure indicator for digital radiography: AAPM Task Group 116 (executive summary)," *Med. Phys.*, vol. 36, no. 7, pp. 2898–2914, Jul. 2009.

[37] P. Tomà, V. Cannatà, E. Genovese, A. Magistrelli, and C. Granata, "Radiation exposure in diagnostic imaging: Wisdom and prudence, but still a lot to understand," *Radiol. Med.*, vol. 122, no. 3, pp. 215–220, Mar. 2017.

[38] D. J. Brenner *et al.*, "Cancer risks attributable to low doses of ionizing radiation: Assessing what we really know," *Proc. Nat. Acad. Sci USA*, vol. 100, no. 24, pp. 13761–13766, Nov. 2003.

[39] A. S. Brody, D. P. Frush, W. Huda, and R. L. Brent, "Radiation risk to children from computed tomography," *Pediatrics*, vol. 120, no. 3, pp. 677–682, Sep. 2007.

[40] Image Gently. (Aug. 8, 2018). *Image Gently Development of Pediatric CT Protocols*. [Online]. Available: http://www.imagegently.org/Portals/6/Procedures/IG%20CT%20Protocols%20111714.pdf

[41] D. P. Frush, B. Soden, K. S. Frush, and C. Lowry, "Improved pediatric multidetector body CT using a size-based color-coded format," *AJR Amer. J. Roentgenol.*, vol. 178, no. 3, pp. 721–726, Mar. 2002.

[42] S. Singh *et al.*, "Dose reduction and compliance with pediatric CT protocols adapted to patient size, clinical indication, and number of prior studies," *Radiology*, vol. 252, no. 1, pp. 200–208, Jul. 2009.

[43] G. I. Ogbole, "Radiation dose in paediatric computed tomography: Risks and benefits," *Ann. IB Postgrad. Med.*, vol. 8, no. 2, pp. 118–126, Dec. 2010.

[44] B. Connolly, J. Racadio, and R. Towbin, "Practice of ALARA in the pediatric interventional suite," *Pediatr. Radiol.*, vol. 36, no. S2, pp. 163–167, 2006.

[45] National Cancer Institute. (Aug. 8, 2018). *Interventional Fluoroscopy: Reducing Radiation Risks for Patients and Staff*. [Online]. Available: http://www.cancer.gov/cancertopics/interventionalfluoroscopy

[46] G. A. Messaris *et al.*, "Hysterosalpingography using a flat panel unit: Evaluation and optimization of ovarian radiation dose," *Med. Phys.*, vol. 39, no. 7, pp. 4404–4413, Jul. 2012.

[47] Image Gently. (Aug. 8, 2018). [Online]. Available: http://www.imagegently.org/Procedures/Interventional-Radiology/StepsforSafetyPedIR

[48] S. Carlson, "A glance at the history of nuclear medicine," *Acta Oncol.*, vol. 34, no. 8, pp. 1095–1102, 1995.

[49] S. T. Treves, *Pediatric Nuclear Medicine/PET*, 3rd ed. New York, NY, USA: Springer, 2007.

[50] S. T. Treves *et al.*, "Nuclear medicine in the first year of life," *J. Nucl. Med.*, vol. 52, no. 6, pp. 905–925, Jun. 2011.

[51] S. C. Chawla *et al.*, "Estimated cumulative radiation dose from PET/CT in children with malignancies: A 5-year retrospective review," *Pediatr. Radiol.*, vol. 40, no. 5, pp. 681–686, May 2010.

[52] American Association of Physicists in Medicine. (2017). *AAPM Position Statement on Radiation Risks From Medical Imaging Procedures: Policy No. PP 25-B*. [Online]. Available: https://www.aapm.org/org/policies/details.asp?id=406&type=PP

[53] Health Physics Society. (Aug. 8, 2018). *Health Physics Society Website. Radiation Risk in Perspective: Position Statement of the Health Physics Society (PS010-1)*. [Online]. Available: https://hps.org/documents/risk_ps010-2.pdf

[54] United Nations Scientific Committee on the Effects of Atomic Radiation, *Report of the United Nations Scientific Committee on the Effects of Atomic Radiation*. New York, NY, USA: UNSCEAR, 2012.

[55] S. T. Treves, A. E. Falone, and F. H. Fahey, "Pediatric nuclear medicine and radiation dose," *Seminar Nucl. Med.*, vol. 44, no. 3, pp. 202–209, May 2014.

[56] M. J. Gelfand, M. T. Parisi, and S. T. Treves, "Pediatric radiopharmaceutical administered doses: 2010 North American consensus guidelines," *J. Nucl. Med.*, vol. 52, no. 2, pp. 318–322, Feb. 2011.

[57] S. T. Treves, M. T. Parisi, and M. J. Gelfand, "Pediatric radiopharmaceutical doses: New guidelines," *Radiology*, vol. 261, no. 2, pp. 347–349, Nov. 2011.

[58] Society of Nuclear Medicine and Molecular Imaging. (Oct. 9, 2018). *Pediatric Injected Activity Tool*. [Online]. Available: http://www.snmmi.org/pedactivitytool

[59] A. Piepsz *et al.*, "A radiopharmaceuticals schedule for imaging in paediatrics. Paediatric Task Group European association nuclear medicine," *Eur. J. Nucl. Med.*, vol. 17, nos. 3–4, pp. 127–129, 1990.

[60] F. Jacobs *et al.*, "Optimised tracer-dependent dosage cards to obtain weight-independent effective doses," *Eur. J. Nucl. Med. Mol. Imag.*, vol. 32, no. 5, pp. 581–588, May 2005.

[61] M. Lassmann *et al.*, "The new EANM paediatric dosage card," *Eur. J. Nucl. Med. Mol. Imag.*, vol. 34, no. 5, pp. 796–798, May 2007.

[62] M. Lassmann *et al.*, "The new EANM paediatric dosage card: Additional notes with respect to F-18," *Eur. J. Nucl. Med. Mol. Imag.*, vol. 35, no. 9, pp. 1666–1668, Sep. 2008.

[63] European Association of Nuclear Medicine. (Oct. 9, 2018). *Dose Calculator*. [Online]. Available: http://www.eanm.org/publications/dosage-calculator/

[64] *PEDDOSE.NET*. Accessed: Oct. 9, 2018. [Online]. Available: https://cordis.europa.eu/result/rcn/55626_en.html

[65] M. Lassmann and S. T. Treves, "Paediatric radiopharmaceutical administration: Harmonization of the 2007 EANM paediatric dosage card (version 1.5.2008) and the 2010 North American consensus guidelines," *Eur. J. Nucl. Med. Mol. Imag.*, vol. 41, no. 5, pp. 1036–1041, May 2014.

[66] S. T. Treves and M. Lassmann, "International guidelines for pediatric radiopharmaceutical administered activities," *J. Nucl. Med.*, vol. 55, no. 6, pp. 869–870, Jun. 2014.

[67] I. Gordon, A. Piepsz, and R. Sixt, "Guidelines for standard and diuretic renogram in children," *Eur. J. Nucl. Med. Mol. Imag.*, vol. 38, no. 6, pp. 1175–1188, Jun. 2011.

[68] B. L. Shulkin *et al.*, "Procedure guideline for diuretic renography in children 3.0," *J. Nucl. Med. Technol.*, vol. 36, no. 3, pp. 162–168, Sep. 2008.

[69] F. D. Grant, M. J. Gelfand, L. A. Drubach, S. T. Treves, and F. H. Fahey, "Radiation doses for pediatric nuclear medicine studies: Comparing the North American consensus guidelines and the pediatric dosage card of the European Association of nuclear medicine," *Pediatr. Radiol.*, vol. 45, no. 5, pp. 706–713, Apr. 2015.

[70] European Association of Nuclear Medicine. (Aug. 8, 2018). [Online]. Available: http://www.eanm.org/docs/EANM_Dosage_Card_040214.pdf

[71] S. T. Treves, M. J. Gelfand, F. H. Fahey, and M. T. Parisi, "2016 Update of the North American consensus guidelines for pediatric administered radiopharmaceutical activities," *J. Nucl. Med.*, vol. 57, no. 12, pp. 15N–18N, Dec. 2016.

[72] F. H. Fahey, S. I. Ziniel, D. Manion, A. Baker, and S. T. Treves, "Administered activities in pediatric nuclear medicine and the impact of the 2010 North American consensus guidelines on general hospitals in the United States," *J. Nucl. Med.*, vol. 57, no. 9, pp. 1478–1485, Sep. 2016.

[73] F. H. Fahey, S. I. Ziniel, D. Manion, and S. T. Treves, "Effects of image gently and the North American guidelines: Administered activities in children at 13 North American pediatric hospitals," *J. Nucl. Med.*, vol. 56, no. 6, pp. 962–967, Jun. 2015.

[74] F. H. Fahey *et al.*, "Standardization of administered activities in pediatric nuclear medicine: A report of the first nuclear medicine global initiative project, part 1-statement of the issue and a review of available resources," *J. Nucl. Med.*, vol. 56, no. 4, pp. 646–651, Apr. 2015.

[75] S. Holm *et al.*, "Paediatric doses—A critical appraisal of the EANM paediatric dosage card," *Eur. J. Nucl. Med. Mol. Imag.*, vol. 34, no. 11, pp. 1713–1718, Nov. 2007.

[76] V. S. Warbey, P. J. Schleyer, S. F. Barrington, and M. J. O'Doherty, "The new EANM paediatric dosage card—Does it conform to ALARA for PET/CT?" *Eur. J. Nucl. Med. Mol. Imag.*, vol. 34, no. 11, pp. 1881–1882, Nov. 2007.

[77] A. T. Taylor *et al.*, "^{99m}Tc-MAG$_3$: Image wisely," *Radiology*, vol. 284, no. 1, pp. 200–209, Jul. 2017.

[78] M. J. Gelfand, "Dose reduction in pediatric hybrid and planar imaging," *Quart. J. Nucl. Med. Mol. Imag.*, vol. 54, no. 4, pp. 379–388, Aug. 2010.

[79] O. Mawlawi, A. Yahil, H. Vija, W. Erwin, and H. Macapinlac, "Reduction in scan duration or injected dose in planar bone scintigraphy enabled by Pixon® post-processing," *J. Nucl. Med.*, vol. 48, no. S2, p. 13P, 2007.

[80] Y. K. Dewaraja *et al.*, "Accurate dosimetry in 131I radionuclide therapy using patient-specific, 3-dimensional methods for SPECT reconstruction and absorbed dose calculation," *J. Nucl. Med.*, vol. 46, no. 5, pp. 840–849, May 2005.

[81] H. Hricak *et al.*, "Managing radiation use in medical imaging: A multifaceted challenge," *Radiology*, vol. 258, no. 3, pp. 889–905, Mar. 2011.

[82] W. Römer *et al.*, "Isotropic reconstruction of SPECT data using OSEM3D: Correlation with CT," *Acad. Radiol.*, vol. 13, no. 4, pp. 496–502, Apr. 2006.

[83] G. R. Small, B. J. Chow, and T. D. Ruddy, "Low-dose cardiac imaging: Reducing exposure but not accuracy," *Expert Rev. Cardiovasc. Therapy*, vol. 10, no. 1, pp. 89–104, Jan. 2012.

[84] A. H. Vija, A. Yahil, and E. G. Hawman, "Adaptive noise reduction and sharpening of OSEM-reconstructed data," presented at the IEEE Nucl. Sci. Symp. Conf. Rec., Oct. 2005.

[85] K. Van Audenhaege *et al.*, "Review of SPECT collimator selection, optimization, and fabrication for clinical and preclinical imaging," *Med. Phys.*, vol. 42, no. 8, pp. 4796–4813, Aug. 2015.

[86] H. Zaidi, "Recent developments and future trends in nuclear medicine instrumentation," *Zeitschrift für Medizinische Physik*, vol. 16, no. 1, pp. 5–17, 2006.

[87] G. C. Kagadis. (Oct. 9, 2018). *ERROR Project: A Pediatric Dosimetry Personalized Platform Based on Computational Anthropomorphic Phantoms*. [Online]. Available: https://error.upatras.gr

[88] T. Kostou, P. Papadimitroulas, G. Loudos, and G. C. Kagadis, "A preclinical simulated dataset of S-values and investigation of the impact of rescaled organ masses using the MOBY phantom," *Phys. Med. Biol.*, vol. 61, no. 6, pp. 2333–2355, Mar. 2016.

[89] P. Papadimitroulas *et al.*, "A personalized, Monte Carlo-based method for internal dosimetric evaluation of radiopharmaceuticals in children," *Med. Phys.*, vol. 45, no. 8, pp. 3939–3949, Jun. 2018.

[90] B. R. Prestidge *et al.*, "Posttreatment biopsy results following interstitial brachytherapy in early-stage prostate cancer," *Int. J. Radiat. Oncol. Biol. Phys.*, vol. 37, no. 1, pp. 31–39, Jan. 1997.

[91] E. A. Healey, R. C. Shamberger, H. E. Grier, J. S. Loeffler, and N. J. Tarbell, "A 10-year experience of pediatric brachytherapy," *Int. J. Radiat. Oncol. Biol. Phys.*, vol. 32, no. 2, pp. 451–455, May 1995.

[92] S. Nag, R. Martinez-Monge, F. B. Ruymann, and C. J. Bauer, "Feasibility of intraoperative high-dose rate brachytherapy to boost low dose external beam radiation therapy to treat pediatric soft tissue sarcomas," *Med. Pediatr. Oncol.*, vol. 31, no. 2, pp. 79–85, Aug. 1998.

[93] C. Chargari *et al.*, "Pulsed-dose rate brachytherapy for pediatric bladder prostate rhabdomyosarcoma: Compliance and early clinical results," *Radiotherapy Oncol.*, vol. 124, no. 2, pp. 285–290, Aug. 2017.

[94] M. R. Folkert *et al.*, "20-year experience with intraoperative high-dose-rate brachytherapy for pediatric sarcoma: Outcomes, toxicity, and practice recommendations," *Int. J. Radiat. Oncol. Biol. Phys.*, vol. 90, no. 2, pp. 362–368, Oct. 2014.

[95] K. A. Goodman *et al.*, "Intraoperative high-dose-rate brachytherapy for pediatric solid tumors: A 10-year experience," *Brachytherapy*, vol. 2, no. 3, pp. 139–146, 2003.

[96] M. Kunz *et al.*, "Early treatment of complex located pediatric low-grade gliomas using iodine-125 brachytherapy alone or in combination with microsurgery," *Cancer Med.*, vol. 5, no. 3, pp. 442–453, Mar. 2016.

[97] S. Laskar *et al.*, "Interstitial brachytherapy for pediatric soft tissue sarcoma: Evolving practice over three decades and long-term outcomes," *Pediatr. Blood Cancer*, vol. 65, no. 9, May 2018, Art. no. e27112.

[98] A. Levy *et al.*, "Late toxicity of brachytherapy after female genital tract tumors treated during childhood: Prospective evaluation with a long-term follow-up," *Radiotherapy Oncol.*, vol. 117, no. 2, pp. 206–212, Nov. 2015.

[99] T. E. Merchant *et al.*, "Brachytherapy for pediatric soft-tissue sarcoma," *Int. J. Radiat. Oncol. Biol. Phys.*, vol. 46, no. 2, pp. 427–432, Jan. 2000.

[100] S. Nag, D. Tippin, and F. B. Ruymann, "Intraoperative high-dose-rate brachytherapy for the treatment of pediatric tumors: The Ohio State University experience," *Int. J. Radiat. Oncol. Biol. Phys.*, vol. 51, no. 3, pp. 729–735, Nov. 2001.

[101] M. I. Ruge *et al.*, "Stereotactic brachytherapy with iodine-125 seeds for the treatment of inoperable low-grade gliomas in children: Long-term outcome," *J. Clin. Oncol.*, vol. 29, no. 31, pp. 4151–4159, Nov. 2011.

[102] W. R. Nelson, H. Hirayama, and D. W. O. Rogers, "The EGS4 code system," Stanford Lin. Accelerator Center, Menlo Park, CA, USA, Rep. SLAC 265, 1985.

[103] J. Halbleib and R. Kensek, *ITS Version 3.0: The Integrated TIGER Series of Coupled Electron/Photon Monte Carlo Transport Codes*. Albuquerque, NM, USA: Sandia Nat. Lab., 1992.

[104] F. Brown, *MCNP—A General Monte Carlo N-Particle Transport Code. Version LA-UR-03-1987*. Los Alamos, NM, USA: Los Alamos Nat. Lab., 2003.

[105] S. Seltzer, "Electron-photon Monte Carlo calculations: The ETRAN code," *Int. J. Radiat. Appl. Instrum. A Appl. Radiat. Isotopes*, vol. 42, no. 10, pp. 917–941, 1991.

[106] J. Sempau, E. Acosta, J. Baro, J. M. Fernández-Varea, and F. Salvat, "An algorithm for Monte Carlo simulation of coupled electron-photon transport," *Nucl. Instrum. Methods Phys. Res. B Beam Int. Mater. Atoms*, vol. 132, no. 3, pp. 377–390, 1997.

[107] J. Sempau, J. Fernandez-Vare, E. Acosta, and F. Salvat, "Experimental benchmarks of the Monte Carlo code penelope," *Nucl. Instrum. Methods Phys. Res. B Beam Int. Mater. Atoms*, vol. 207, no. 2, pp. 107–123, 2003.

[108] S. Agostinelli *et al.*, "Geant4—A simulation toolkit," *Nucl. Instrum. Methods Phys. Res. A Accelerators Spectr. Detectors Assoc. Equ.*, vol. 506, no. 3, pp. 250–303, 2003.

[109] (Oct. 9, 2018). *Geant4*. [Online]. Available: http://geant4.cern.ch/

[110] S. Jan *et al.*, "GATE: A simulation toolkit for PET and SPECT," *Phys. Med. Biol.*, vol. 49, no. 19, p. 18, 2004.

[111] J. Bert, D. Benoit, M. Garcia, and D. Visvikis, "GGEMS: GPU GEant4-based Monte Carlo simulation platform," in *Proc. IEEE Nucl. Sci. Symp. Med. Imag. Conf.*, 2016.

[112] P. Arce, P. Rato, M. Canadas, and J. I. Lagares, "GAMOS: A Geant4-based easy and flexible framework for nuclear medicine applications," in *Proc. IEEE Nucl. Sci. Symp. Conf. Rec.*, Dresden, Germany, 2008, pp. 3162–3168.

[113] J. Perl, J. Shin, J. Schümann, B. Faddegon, and H. Paganetti, "TOPAS: An innovative proton Monte Carlo platform for research and clinical applications," *Med. Phys.*, vol. 39, no. 11, pp. 6818–6837, 2012.

[114] T. Akagi *et al.*, "The PTSim and TOPAS projects, bringing Geant4 to the particle therapy clinic," *Progr. Nucl. Sci. Technol.*, vol. 2, pp. 912–917, Oct. 2011.

[115] (Oct. 9, 2018). *OpenGATE Collaboration*. [Online]. Available: http://www.opengatecollaboration.org

[116] (Oct. 9, 2018). *GGEMS*. [Online]. Available: http://ggems.fr/

[117] R. Straton *et al.*, "Organ and effective doses in newborn patients during helical multislice computed tomography examination," *Phys. Med. Biol.*, vol. 51, no. 20, p. 15, 2006.

[118] C. Lee *et al.*, "Organ and effective doses in pediatric patients undergoing helical multislice computed tomography examination," *Radiat. Protect. Phys.*, vol. 34, no. 5, p. 15, 2007.

[119] X. Li *et al.*, "Patient-specific radiation dose and cancer risk for pediatric chest CT," *Radiology*, vol. 259, no. 3, p. 12, 2011.

[120] X. Tian *et al.*, "Pediatric chest and abdominopelvic CT: Organ dose estimation based on 42 patient models," *Radiology*, vol. 270, no. 2, p. 12, 2014.

[121] J. Gu, B. Bednarz, P. Caracappa, and X. Xu, "The development, validation and application of a multi-detector CT (MDCT) scanner model for assessing organ doses to the pregnant patient and the fetus using Monte Carlo simulations," *Phys. Med. Biol.*, vol. 54, no. 9, pp. 2699–2717, 2009.

[122] H. Schlattl, M. Zankl, J. Becker, and C. Hoeschen, "Dose conversion coefficients for paediatric CT examinations with automatic tube current modulation," *Phys. Med. Biol.*, vol. 57, no. 20, p. 17, 2012.

[123] S. Kost *et al.*, "Patient-specific dose calculations for pediatric CT of the chest, abdomen and pelvis," *Pediatr. Radiol.*, vol. 45, no. 12, pp. 1771–1780, 2015.

[124] S. Marcatili, D. Villoing, T. Mauxion, B. J. McParland, and M. Bardiès, "Model-based versus specific dosimetry in diagnostic context: Comparison of three dosimetric approaches," *Med. Phys.*, vol. 42, no. 3, pp. 1288–1296, 2015.

[125] J. Grimes and A. Celler, "Comparison of internal dose estimates obtained using organ-level, voxel S value, and Monte Carlo techniques," *Med. Phys.*, vol. 41, no. 9, 2014, Art. no. 092501.

[126] E. E. Furhang, C. S. Chui, K. S. Kolbert, S. M. Larson, and G. Sgouros, "Implementation of a Monte Carlo dosimetry method for patient-specific internal emitter therapy," *Med. Phys.*, vol. 24, no. 7, pp. 1163–1172, 1997.

[127] C. Champion, P. Zanotti-Fregonara, and E. Hindié, "CELLDOSE: A Monte Carlo code to assess electron dose distribution—S-values for 131I in spheres of various sizes," *Nucl. Med.*, vol. 49, no. 1, pp. 151–157, 2008.

[128] S. Chiavassa *et al.*, "OEDIPE: A personalized dosimetric tool associating voxel-based models with MCNPX," *Cancer Biotherapy Radiopharmaceuticals*, vol. 20, no. 3, pp. 325–332, 2005.

[129] M.-A. Descalle *et al.*, "Application of MINERVA Monte Carlo simulations to targeted radionuclide therapy," *Cancer Biotherapy Radiopharmaceuticals*, vol. 18, no. 1, pp. 71–79, 2003.

[130] *Welcome to RADAR—The RAdiation Dose Assessment Resource*. Accessed: Oct. 9, 2018. [Online]. Available: http://www.doseinfo-radar.com/RADARHome.html

[131] X. Liu, M. Ljungberg, and S.-E. Strand, "DOSIMG: A 3D voxel-based Monte Carlo program for absorbed dose calculations," *J. Nucl. Med.*, vol. 42, p. 243P, 2001.

[132] A. R. Prideaux *et al.*, "Three-dimensional radiobiologic dosimetry: Application of radiobiologic modeling to patient-specific 3-dimensional imaging-based internal dosimetry," *Nucl. Med.*, vol. 48, no. 6, pp. 1008–1016, 2007.

[133] S. J. Wilderman and Y. K. Dewaraja, "Method for fast CT/SPECT-based 3D Monte Carlo absorbed dose computations in internal emitter therapy," *IEEE Trans. Nucl. Sci.*, vol. 54, no. 1, pp. 146–151, Feb. 2007.

[134] M. Wayson *et al.*, "Internal photon and electron dosimetry of the newborn patient—A hybrid computational phantom study," *Phys. Med. Biol.*, vol. 57, no. 5, pp. 1433–1457, Mar. 2012.

[135] T. Xie, W. E. Bolch, C. Lee, and H. Zaidi, "Pediatric radiation dosimetry for positron-emitting radionuclides using anthropomorphic phantoms," *Med. Phys.*, vol. 40, no. 10, Oct. 2013, Art. no. 102502.

[136] H. Yoriyaz, M. G. Stabin, and A. dos Santos, "Monte Carlo MCNP-4B-based absorbed dose distribution estimates for patient-specific dosimetry," *J. Nucl. Med.*, vol. 42, no. 4, pp. 662–669, Apr. 2001.

[137] A. V. Gil, M. A. C. Perez, L. A. T. Aroche, and M. Pacilio, "MCID: Herramienta dosimetrica personalizada para simular estudios voxelizados con MCNP5," presented at the IX Latin Amer. IRPA Reg. Congr. Radiat. Protect. Safety (IRPA), Rio de Janeiro, Brazil, Apr. 2013.

[138] F. Botta *et al.*, "Use of the FLUKA Monte Carlo code for 3D patient-specific dosimetry on PET-CT and SPECT-CT images," *Phys. Med. Biol.*, vol. 58, no. 22, pp. 8099–8120, Nov. 2013.

[139] S. D. Kost, Y. K. Dewaraja, R. G. Abramson, and M. G. Stabin, "VIDA: A voxel-based dosimetry method for targeted radionuclide therapy using Geant4," *Cancer Biotherapy Radiopharmaceuticals*, vol. 30, no. 1, pp. 16–26, Feb. 2015.

[140] S. Marcatili *et al.*, "Development and validation of RAYDOSE: A Geant4-based application for molecular radiotherapy," *Phys. Med. Biol.*, vol. 58, no. 8, pp. 2491–2508, Apr. 2013.

[141] M. D. Belley *et al.*, "Toward an organ based dose prescription method for the improved accuracy of murine dose in orthovoltage X-ray irradiators," *Med. Phys.*, vol. 41, no. 3, Mar. 2014, Art. no. 034101.

[142] L. Ferrer, N. Chouin, A. Bitar, A. Lisbona, and M. Bardies, "Implementing dosimetry in GATE: Dose-point kernel validation with GEANT4 4.8.1," *Cancer Biotherapy Radiopharmaceuticals*, vol. 22, no. 1, pp. 125–129, Feb. 2007.

[143] M. Momennezhad *et al.*, "A 3D Monte Carlo method for estimation of patient-specific internal organs absorbed dose for (99m)Tc-hynic-Tyr(3)-octreotide imaging," *World J. Nucl. Med.*, vol. 15, no. 2, pp. 114–123, May/Aug. 2016.

[144] A. A. Parach, H. Rajabi, and M. A. Askari, "Paired organs-should they be treated jointly or separately in internal dosimetry?" *Med. Phys.*, vol. 38, no. 10, pp. 5509–5521, Oct. 2011.

[145] A. A. Parach, H. Rajabi, and M. A. Askari, "Assessment of MIRD data for internal dosimetry using the GATE Monte Carlo code," *Radiat. Environ. Biophys.*, vol. 50, no. 3, pp. 441–450, Aug. 2011.

[146] E. Saeedzadeh *et al.*, "3D calculation of absorbed dose for 131I-targeted radiotherapy: A Monte Carlo study," *Radiat. Protect. Dosimetry*, vol. 150, no. 3, pp. 298–305, Jul. 2012.

[147] D. Visvikis *et al.*, "Use of the GATE Monte Carlo package for dosimetry applications," *Nucl. Instrum. Methods Phys. Res. A Accelerators Spect Detectors Assoc. Equ.*, vol. 569, no. 2, pp. 335–340, 2006.

[148] Y. Jia *et al.*, "Proton therapy dose distribution comparison between Monte Carlo and a treatment planning system for pediatric patients with ependymoma," *Med. Phys.*, vol. 39, no. 8, pp. 4742–4747, 2012.

[149] K. Chatzipapas, P. Papadimitroulas, G. Loudos, N. Papanikolaou, and G. Kagadis, "SUF-T-50: Evaluation of Monte Carlo simulations performance for pediatric brachytherapy dosimetry," *Med. Phys.*, vol. 43, no. 6, pp. 3472–3473, 2016.

[150] *Report of Committee II on Permissible Dose for Internal Radiation*, ICRP, Ottawa, ON, Canada, 1959.

[151] W. Snyder, M. R. Ford, G. G. Warner, and H. L. Fisher, Jr., "Estimates of absorbed fractions for monoenergetic photon sources uniformly distributed in various organs of a heterogeneous phantom," *Nucl. Med.*, vol. 5, no. S3, pp. 7–52, 1969.

[152] "Report on the task group on reference man," ICRP, Ottawa, ON, Canada, Rep. e23, p. 480, 1975.

[153] R. Loevinger, T. Budinger, and E. Watson, *MIRD Primer for Absorbed Dose Calculations*. New York, NY, USA: Soc. Nucl. Med., 1988.

[154] M. Cristy and K. Eckerman, "Specific absorbed fractions of energy at various ages from internal photon sources," Dept. Metabolism Dosimetry Res. Group, Oak Ridge Nat. Lab., Oak Ridge, TN, USA, Rep. ORNL/TM-8381/V1-V7, 1987.

[155] M. Stabin, "MIRDOSE—The personal computer software for use in internal dose assessment in nuclear medicine," *Nucl. Med.*, vol. 37, no. 3, pp. 538–546, 1996.

[156] C. Lee, J. L. Williams, C. Lee, and W. E. Bolch, "The UF series of tomographic computational phantoms of pediatric patients," *Med. Phys.*, vol. 32, no. 12, pp. 3537–3548, 2005.

[157] A. M. Geyer, S. O'Reilly, C. Lee, D. J. Long, and W. E. Bolch, "The UF/NCI family of hybrid computational phantoms representing the current U.S. population of male and female children, adolescents, and adults—Application to CT dosimetry," *Phys. Med. Biol.*, vol. 59, no. 18, pp. 5225–5242, Sep. 2014.

[158] X. Xu, T. Chao, and A. Bozkurt, "VIP-Man: An image-based whole-body adult male model constructed from color photographs of the visible human project for multi-particle Monte Carlo calculations," *Health Phys.*, vol. 78, no. 5, pp. 476–486, 2000.

[159] H. Norris *et al.*, "A set of 4D pediatric XCAT reference phantoms for multimodality research," *Med. Phys.*, vol. 41, no. 3, 2014, Art. no. 033701.

[160] A. Christ *et al.*, "The virtual family—Development of surface-based anatomical models of two adults and two children for dosimetric simulations," *Phys. Med. Biol.*, vol. 55, no. 2, pp. N23–N38, 2010.

[161] D. E. Carver *et al.*, "Realistic phantoms to characterize dosimetry in pediatric CT," *Pediatr. Radiol.*, vol. 47, no. 6, pp. 691–700, 2017.

[162] T. Xie, N. Kuster, and H. Zaidi, "Computational hybrid anthropometric paediatric phantom library for internal radiation dosimetry," *Phys. Med. Biol.*, vol. 62, no. 8, pp. 3263–3283, Apr. 2017.

[163] P. Papadimitroulas, Y. Kopsinis, D. Karnabatidis, and G. Kagadis, "Monte Carlo based platform for peronalixed pediatric dosimetry in nuclear medicine applications," presented at the RSNA 103rd Sci. Assembly Annu. Meeting, Chicago, IL, USA, 2017. [Online]. Available: http://archive.rsna.org/2017/PhysicsandBasicScience.pdf

[164] S. Theodoridis, *Machine Learning*. New York, NY, USA: Academic, 2015.

[165] K. K. Roy and A. Phadikar, "Automated medical image segmentation: A survey," in *Proc. Int. Conf. Comput. Commun. Manuf.*, vol. 1, 2014, pp. 1–5.

[166] R. P. Burke *et al.*, "Multi-atlas segmentation for abdominal organs with Gaussian mixture models," in *Proc. SPIE Int. Soc. Opt. Eng.*, vol. 9417, Mar. 2015, Art. no. 941707.

[167] C. Chu, J. Bai, X. Wu, and G. Zheng, "MASCG: Multi-atlas segmentation constrained graph method for accurate segmentation of hip CT images," *Med. Image Anal.*, vol. 26, no. 1, pp. 173–184, Dec. 2015.

[168] M. Oda *et al.*, "Regression forest-based atlas localization and direction specific atlas generation for pancreas segmentation," in *Proc. Int. Conf. Med. Image Comput. Comput. Assist. Intervent.*, 2016, pp. 556–563.

[169] T. Okada *et al.*, "Abdominal multi-organ segmentation from CT images using conditional shape-location and unsupervised intensity priors," *Med. Image Anal.*, vol. 26, no. 1, pp. 1–18, Dec. 2015.

[170] E. Schreibmann, D. M. Marcus, and T. Fox, "Multiatlas segmentation of thoracic and abdominal anatomy with level set-based local search," *J. Appl. Clin. Med. Phys.*, vol. 15, no. 4, p. 4468, Jul. 2014.

[171] T. Tong *et al.*, "Discriminative dictionary learning for abdominal multi-organ segmentation," *Med. Image Anal.*, vol. 23, no. 1, pp. 92–104, Jul. 2015.

[172] Z. Xu *et al.*, "Efficient multi-atlas abdominal segmentation on clinically acquired CT with SIMPLE context learning," *Med. Image Anal.*, vol. 24, no. 1, pp. 18–27, Aug. 2015.

[173] J. Zhou *et al.*, "Automated compromised right lung segmentation method using a robust atlas-based active volume model with sparse shape composition prior in CT," *Comput. Med. Imag. Graph.*, vol. 46, pp. 47–55, Dec. 2015.

[174] J. J. Cerrolaza, M. Reyes, R. M. Summers, M. A. González-Ballester, and M. G. Linguraru, "Automatic multi-resolution shape modeling of multi-organ structures," *Med. Image Anal.*, vol. 25, no. 1, pp. 11–21, Oct. 2015.

[175] T. Heimann and H.-P. Meinzer, "Statistical shape models for 3D medical image segmentation: A review," *Med. Image Anal.*, vol. 13, no. 4, pp. 543–563, Aug. 2009.

[176] C. P. Lee *et al.*, "Evaluation of five image registration tools for abdominal CT: Pitfalls and opportunities with soft anatomy," in *Proc. SPIE Int. Soc. Opt. Eng.*, 2015, p. 9413.

[177] Y. LeCun, Y. Bengio, and G. Hinton, "Deep learning," *Nature*, vol. 521, no. 7553, pp. 436–444, May 2015.

[178] G. Litjens *et al.*, "A survey on deep learning in medical image analysis," *Med. Image Anal.*, vol. 42, pp. 60–88, Dec. 2017.

[179] J. Long, E. Shelhamer, and T. Darrell, "Fully convolutional networks for semantic segmentation," in *Proc. IEEE CVPR*, Boston, MA, USA, 2015, pp. 3431–3440.

[180] O. Ronneberger, P. Fischer, and T. Brox, "U-Net: Convolutional networks for biomedical image segmentation," presented at the Lecture Notes Comput. Sci., 2015.
[181] O. Çiçek, A. Abdulkadir, S. S. Lienkamp, T. Brox, and O. Ronneberger, "3D U-Net: Learning dense volumetric segmentation from sparse annotation," in *Proc. Int. Conf. Med. Image Comput. Comput. Assist. Intervent.*, 2016, pp. 424–432.
[182] F. Milletari, N. Navab, and S. A. Ahmadi, "V-Net: Fully convolutional neural networks for volumetric medical image segmentation," *arXiv 1606.04797 [cs]*, 2016.
[183] H. R. Roth *et al.*, "Deep learning and its application to medical image segmentation," *arXiv 1803.08691 [cs]*, 2018.
[184] E. Gibson *et al.*, "Towards image-guided pancreas and biliary endoscopy: Automatic multi-organ segmentation on abdominal CT with dense dilated networks," presented at the MICCAI, 2017.
[185] E. Gibson *et al.*, "Automatic multi-organ segmentation on abdominal CT with dense V-networks," *IEEE Trans. Med. Imag.*, vol. 37, no. 8, pp. 1822–1834, Aug. 2018.
[186] G. Huang, Z. Liu, K. Q. Weinberger, and L. van der Maaten, "Densely connected convolutional networks," *arXiv 1608.06993*, 2016.
[187] X. Zhou *et al.*, "Three-dimensional CT image segmentation by combining 2D fully convolutional network with 3D majority voting," in *Proc. MICCAI Workshop Large Scale Annotation Biomed. Data Exp. Label Synth.*, 2016, pp. 111–120.
[188] E. Gibson *et al.*, "NiftyNet: A deep-learning platform for medical imaging," *Comput. Methods Prog. Biomed.*, vol. 158, pp. 113–122, May 2018.
[189] W. Dai *et al.*, "SCAN: Structure correcting adversarial network for organ segmentation in chest X-rays," *arXiv 1703.08770*, 2017.
[190] B. Ibragimov and L. Xing, "Segmentation of organs-at-risks in head and neck CT images using convolutional neural networks," *Med. Phys.*, vol. 44, no. 2, pp. 547–557, Feb. 2017.
[191] P. Jackson *et al.*, "Deep learning renal segmentation for fully automated radiation dose estimation in unsealed source therapy," *Front. Oncol.*, vol. 8, p. 215, Jun. 2018.
[192] T. Lustberg *et al.*, "Clinical evaluation of atlas and deep learning based automatic contouring for lung cancer," *Radiotherapy Oncol.*, vol. 126, no. 2, pp. 312–317, Feb. 2018.
[193] K. Men, J. Dai, and Y. Li, "Automatic segmentation of the clinical target volume and organs at risk in the planning CT for rectal cancer using deep dilated convolutional neural networks," *Med. Phys.*, vol. 44, no. 12, pp. 6377–6389, Dec. 2017.
[194] W. Fu *et al.*, "From patient-informed to patient-specific organ dose estimation in clinical computed tomography," presented at the Med. Imag. Phys. Med. Imag., Houston, TX, USA, 2018.
[195] J. Cho *et al.*, "Machine Learning powered automatic organ classification for patient specific organ dose estimation," presented at the Soc. Imag. Informat. Med., 2017.
[196] X. Tian, W. P. Segars, R. L. Dixon, and E. Samei, "Convolution-based estimation of organ dose in tube current modulated CT," *Phys. Med. Biol.*, vol. 61, no. 10, pp. 3935–3954, May 2016.
[197] (Aug. 25, 2018). *GE Healthcare to License Duke University's CT Organ Dosimetry Technology*. [Online]. Available: https://www.genewsroom.com/press-releases/ge-healthcare-license-duke-university's-ct-organ-dosimetry-technology-284259
[198] X. G. Xu, "An exponential growth of computational phantom research in radiation protection, imaging, and radiotherapy: A review of the fifty-year history," *Phys. Med. Biol.*, vol. 59, no. 18, pp. R233–R302, Sep. 2014.
[199] E. L. Marshall, D. Borrego, T. Tran, J. C. Fudge, and W. E. Bolch, "Evaluation of the UF/NCI hybrid computational phantoms for use in organ dosimetry of pediatric patients undergoing fluoroscopically guided cardiac procedures," *Phys. Med. Biol.*, vol. 63, no. 5, Mar. 2018, Art. no. 055006.
[200] E. J. Stepusin, D. J. Long, E. L. Marshall, and W. E. Bolch, "Assessment of different patient-to-phantom matching criteria applied in Monte Carlo-based computed tomography dosimetry," *Med. Phys.*, vol. 44, no. 10, pp. 5498–5508, Oct. 2017.
[201] E. Neufeld, A. M. Cassara, H. Montanaro, N. Kuster, and W. Kainz, "Functionalized anatomical models for EM-neuron interaction modeling," *Phys. Med. Biol.*, vol. 61, no. 12, pp. 4390–4401, Jun. 2016.
[202] S. Pollock, J. Kipritidis, D. Lee, K. Bernatowicz, and P. Keall, "The impact of breathing guidance and prospective gating during thoracic 4DCT imaging: An XCAT study utilizing lung cancer patient motion," *Phys. Med. Biol.*, vol. 61, no. 17, pp. 6485–6501, Sep. 2016.
[203] B. Lloyd *et al.*, "Covering population variability: Morphing of computation anatomical models," in *Simulation and Synthesis in Medical Imaging*, S. A. Tsaftaris, A. Gooya, A. F. Frangi, and J. L. Prince, Eds. Cham, Switzerland: Springer Int., 2016, pp. 13–22.
[204] Z. Cai, J. P. Pignol, C. Chan, and R. M. Reilly, "Cellular dosimetry of (111)In using Monte carlo N-particle computer code: Comparison with analytic methods and correlation with in vitro cytotoxicity," *J. Nucl. Med.*, vol. 51, no. 3, pp. 462–470, Mar. 2010.
[205] R. Freudenberg and J. Kotzerke, "Cellular dosimetry using the Geant4 Monte Carlo toolkit," *J. Nucl. Med.*, vol. 51, no. 9, pp. 1488–1489, Sep. 2010.
[206] S. Incerti, M. Douglass, S. Penfold, S. Guatelli, and E. Bezak, "Review of Geant4-DNA applications for micro and nanoscale simulations," *Phys. Med.*, vol. 32, no. 10, pp. 1187–1200, Oct. 2016.